Dental zirconia fabricated by stereolithography: Accuracy, translucency and mechanical properties in different build orientations

Dong Xiang [a,b,c], Yongxiang Xu [a,b,c], Wei Bai [a,b,c], Hong Lin [a,b,c,*]

[a] Department of Dental Materials, Peking University School and Hospital of Stomatology, Beijing, 100081, PR China
[b] NMPA Key Laboratory for Dental Materials & Dental Medical Devices Testing Center, Peking University School of Stomatology, Beijing, 100081, PR China
[c] National Engineering Laboratory for Digital and Material Technology of Stomatology & National Clinical Research Center for Oral Diseases & Beijing Key Laboratory of Digital Stomatology, Peking University School and Hospital of Stomatology, Beijing, 100081, PR China

ARTICLE INFO

ABSTRACT

Additive manufacturing (AM) zirconia shows excellent prospects for use in clinical applications. In this work, AM zirconia samples were fabricated in horizontal (H) and upright (U) fashion using a stereolithography appearance (SLA) system. The dimensional accuracy, density, translucency, surface quality, flexural strength and fracture toughness (K_{Ic}) of the samples were then assessed. AM zirconia fabricated in a H fashion shows excellent dimensional accuracy. Samples fabricated in a U fashion exhibit a higher density (relative density 95.4%) and translucency (4.393), but H group samples exhibit a higher K_{Ic} value (12.635 $\pm$ 1.372 MPa m$^{1/2}$). The flexural strengths of the samples were measured and the values were compared according to their different build orientations, surface quality and fracture modes. Manual defects that arose in the samples as a result of their separation from the build platform in which they were made were found to lead to samples with irregular surface morphologies and increased surface roughness. However, this type of defect does not affect the flexural strength of samples fabricated in a H fashion. Polished-H samples that fracture from the stress concentration area exhibit the highest flexural strength (1151.08 $\pm$ 166.41 MPa) amongst all the samples prepared in this work. However, the flexural strength of the samples prepared in a U fashion is obviously low, even after polishing (225.44 $\pm$ 46.10 MPa). The Weibull characteristic strengths and Weibull moduli of the as-sintered samples are 920.22 MPa and 6.50 for H and 219.59 MPa and 7.99 for U, respectively. Overall, it was found that the dimensional accuracy, density, translucency, surface quality and mechanical properties of materials vary according to their different build orientations.

1. Introduction

Among the large number of reported all-ceramic framework materials, zirconia has the best mechanical properties [1]. The methods of fabricating ceramics with desirable properties and complex geometries are still inefficient and require a high amount of energy [2]. Simple zirconia blocks can be made into ceramic parts with complex shapes that are commonly used in dentistry via traditional computer-aided design and computer-aided manufacturing (CAD/CAM), but there are drawbacks in this method due to the limitations of the diameter of the cutting head in the manufacturing process, as well as the brittleness and hardness of zirconia. In the CAD/CAM process, approximately 90% of a prefabricated block is removed in the fabrication of a typical dental restoration object, generating an enormous amount of materials waste

[3].

As opposed to subtractive manufacturing, additive manufacturing (AM), also known as three-dimensional (3D) printing, is a process that generates a minimal amount of waste, and it has been used to fabricate complex and high-precision materials [4]. AM techniques have been successfully used to print resin and metal crowns, metal dentures and implants [5–12]. AM has also been used to fabricate ceramics via stereolithography appearance (SLA), which is a photocuring AM technique [4]. SLA-fabricated ceramics are free from geometric restrictions, meaning that they meet the requirements for producing customised dental prostheses [13]. Compared with other AM techniques, SLA can not only be used to make materials with a smoother surface finish, but also improve the precision of their production [2]. The construction process proceeds via a layer-by-layer principle, via a photochemical
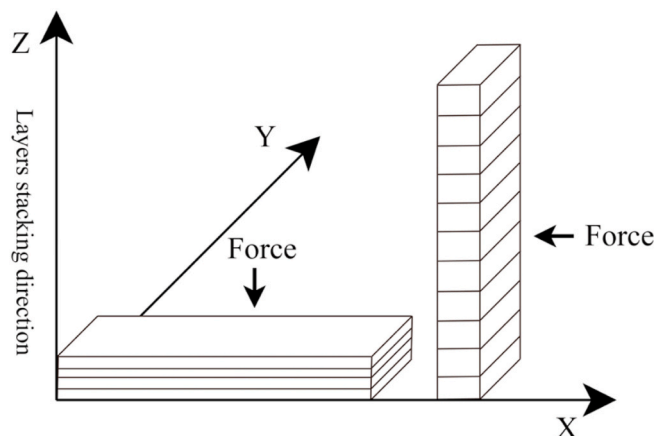

Fig. 1. A sketched map of the samples, in which the Z axis represents the build orientation, i.e., the layers stacking direction. Force was applied on 4×22 mm^2 faces in the three-point bending tests.

reaction wherein a photosensitive liquid polymer is cured as the model is built [14]. The cross-linked structure provides the green body of the material with mechanical strength. After production, post heat-treatment is an important process that is carried out to ensure the quality of AM zirconia. A binder burnout heat-treatment process ensures that any organics in the produced material are decomposed and evaporated off. Thermogravimetric analysis is often used to monitor the change in quality of a material during the heat-treatment process and the de-binding procedure is designed according to the analysis: in temperature ranges in which the quality is slowly lost, the heating rate of the de-binding process can be increased to save time; but when the quality rapidly declines, a slower heating rate can be used to ensure that fewer defects are created in the product being measured [15]. The binder-free object is then sintered to produce a dense material [16].

However, unlike the relatively mature manufacturing processes of polymers and alloys, the fabrication of ceramics via AM is still in its initial stages and many challenges still remain in this area [17,18]. These challenges include, but are not limited to, surface quality, dimensional accuracy and the mechanical properties of the final printed objects [19,20]. Previous studies focused on the accuracy of the printed objects. Zirconia implants fabricated via digital light processing have been proven to have sufficient dimensional accuracy [19]. Zirconia crowns produced via SLA have also been shown to meet surface trueness requirements [21]. Superior to CAD/CAM zirconia, AM zirconia exhibits outstanding reproduction of sharp-edged crown margins, as well as exact reproduction of the occlusal surfaces with sharp and natural replication of fissures [1]. AM zirconia can not only be used to produce monolithic crowns or implants, but also has potential for use as substrates. AM zirconia has been proven to exhibit adequate bond strength when veneered with dental porcelains [22].

However, in the manufacturing of AM monolithic ceramics, enabling the components to achieve a dense part that fully retains their superior physicochemical properties, is still a challenge and remains an important issue that needs to be solved for them to be used in practical applications [17]. AM ceramics when constructed in different orientations can exhibit poor mechanical properties. As shown in Fig. 1, horizontally printed (long axis parallel to the build platform and load perpendicular to the layers) objects exhibit significantly higher strength than those printed upright (long axis perpendicular to the build platform and load parallel to the layers) [19,23]. However, this phenomenon needs to be discussed and studied in detail before the practical use of materials printed in this way. A disadvantage of the use of zirconia as a material in manufacturing is its aesthetics, as it exhibits poor translucency [24]. Therefore, it is necessary to investigate the translucency of AM zirconia in different build orientations. When printing complex-shaped crowns,

supports are added on occlusal surfaces as this region is not easily broken by separation forces and can be easily adjusted to ensure precision [25]. However, surface defects (manual defects) arise when objects are manually separated from supports or the build platform on which they are prepared. In this regard, there is a lack of research on the effect that manual defects have on the flexural strength of manufactured objects. According to previous studies, the shrinkage rates of different orientations are not the same, which may lead to diverse dimensional accuracy and difficulty in controlling precision [13,26]. Dimensional accuracy is an essential property of AM zirconia for its use in applications and should therefore be investigated.

With the above in mind, the objectives of this research were (1) to investigate the dimensional accuracy, translucency and mechanical properties of AM zirconia in different build orientations and (2) to investigate the effect that manual defects have on its flexural strength. The null hypotheses are that the dimensional accuracy, translucency and mechanical properties are the same in different build orientations, and that manual defects have no effect on the flexural strength of AM zirconia.

2. Materials and methods

2.1. Sample preparation

Short bars (3 mm in thickness, 4 mm in width, 22 mm in length) and long bars (3 mm in width, 4 mm in thickness, 36 mm in length) of zirconia were constructed in two orientations; they were printed in a horizontal (H, short bars laying on 4×22 mm^2 faces and long bars laying on 4×36 mm^2 faces) and upright (U, laying on 3×4 mm^2 faces) fashion using a 3D printer (CSL 100, Porimy 3D printing Technology, Kunshan, China). Short bars were used to measure the dimensional accuracy, density, surface quality and flexural strength of the samples. Long bars were used in fracture toughness testing. Discs (15 mm in diameter and 1 mm in thickness) were printed as previously mentioned to measuring their translucency (H: diameter horizontal to the build orientation, U: diameter parallel to the build orientation). CAD/CAM (C) discs and long bars (D98-20, Upcera, China) with the same dimensions as the SLA samples were prepared and their translucency and fracture toughness were measured.

The slurry used in the SLA process was composed of a 16 wt% photosensitive resin mixture comprising 1,6-hexanediol diacrylate and 4.5–6.5 wt% Y$_2$O$_3$-stabilised zirconia at a concentration of 84 wt%. This photosensitive resin was then cured under an ultraviolet light source with a wavelength of 355 nm, where the layer height was 25 μm, the scan speed was 2000 mm/s, the scan space was 25 μm, and the spot diameter was 50 μm. A standard alternating x/y-raster scanning pattern was adopted in each layer of the curing process.

The build platform was in the vat, leaving only a small gap of 25 μm from the liquid level of the slurry, which corresponds to the layer thickness. A primary layer was cured on the build platform upon which the follow-up parts could stably attach. The build platform was lowered by 25 μm after the curing of the previous layer, and the cured surface was then re-coated with ceramic suspension. The green parts were layer-by-layer constructed, with this process being repeated until the target objects were fully formed. The objects were formed in an oversized manner to compensate for the shrinkage that occurs in the subsequent post heat-treatment process. After the SLA process was completed, the green parts were removed from the build platform, which led to the formation of two surfaces that have different morphologies: with the final cured surfaces representing the initial condition (S1) and surfaces attached to the build platform, which may have manual defects (S2). For the sample group with U build orientation, the side faces of the samples when subjected to tensile stress in three-point bending tests only exhibit one state (S3). The green parts were ultrasonically cleaned using ethanol, before being subjected to a binder burnout process at 550 °C and sintering at 1500 °C for 2 h to produce dense parts.

2.2. Dimensional accuracy measurements

The dimensions of short bars (n = 15 per orientation) were measured three times using a caliper, from which mean values were calculated and compared with theoretical dimensions (3 mm in thickness, 4 mm in width, 22 mm in length) using a one-sample *t*-test.

2.3. X-ray diffraction (XRD) measurements

The crystalline phase of the H and U groups of samples were characterised by XRD (Ultima IV, Rigaku, Japan) over a 10–80° diffraction angle range.

2.4. Density measurements

The densities of the H and U (n = 7 per orientation) groups of samples were determined using short bars via the Archimedes method. Data were normalised and homogeneous, and statistical analysis was carried out using an independent-samples *t*-test.

2.5. Translucency measurements

To carry out translucency measurements, disc samples (n = 5 per orientation) were fabricated as previously described. Spectral transmittance (%T) data were collected at 1 nm intervals in the wavelength range of 400–760 nm using an ultraviolet spectrophotometer (CARY 300, Agilent, US), with each disc measured twice. The %T without a sample in the optical path was recorded as the baseline. The average values of %T (sum of %T at each wavelength divided by the number of data points) were calculated to determine the translucency of the samples [27].

2.6. Surface quality measurements

The surfaces of short bars were observed using an optical microscope. The arithmetic average of the absolute values of the profile heights over the evaluation length (*R*a values) of S1 (n=8), S2 (n=7) and S3 (n=6) were measured using a profilometer (SJ-400, Mitutoyo, Japan), the data of which showed normality and homogeneity of variance. One-way analysis of variance (ANOVA) was used to compare *R*a values, and least significant difference (LSD) post hoc tests were carried out to make comparisons between the groups.

2.7. Flexural strength (σ) measurements, fracture surface observations and Weibull statistics

Short bars were selected for three-point bending tests using a universal mechanical testing machine (5969, Instron, US) with a crosshead speed of 1.0 mm/min and a span of 20 mm. For short bars of the H group (n = 21), the as-sintered samples (As–H, n = 15) were divided into two subgroups according to the surfaces set as the tensile side: S1 (H1, n = 8) and S2 (H2, n = 7). Short bars of the H group with surfaces polished to 2000 grit diamond (Polished-H, n = 6) were also tested. Samples of the H group were regrouped and analysed according to their fracture modes and surface quality, which will be discussed in detail in section 3.4.

For short bars of the U group (n = 20), the as-sintered samples set with S3 as the tensile side (As–U, n = 16) and samples polished to 2000 grit diamond (Polished-U, n = 4) were tested.

For the group H, analysis was carried out using one-way ANOVA and LSD post hoc was used to make comparisons between the groups. Independent-samples t-tests were used to compare the As–U and Polished-U samples.

After conducting three-point bending tests, the fracture surfaces of the as-sintered short bars were observed using scanning electron microscopy (SEM, EVO 18, ZEISS, Germany) after sputtering the samples with gold.

Table 1
Means and standard deviations (SDs) of the dimensions, units: mm.

Group	Quantity	Thickness	Width	Length
H	15	2.98 (±0.043)	3.96 (±0.005)[a]	21.97 (±0.049)[a]
U	16	2.94 (±0.022)[a]	3.96 (±0.009)[a]	22.23 (±0.104)[a]

[a] Represents statistically significant differences from the theoretical dimensions.

The numbers of As–H (H1 and H2) and As–U samples were 15 and 16, respectively. Only these two groups met Weibull statistics requirements in terms of numbers of samples (n ≥ 15). The Weibull modulus (m) and Weibull characteristic strength (σ_0) were calculated to assess the structural reliability of the AM zirconia samples.

2.8. Fracture toughness (K_{Ic}) measurements

The single-edge V-Notch Beam (SEVNB) method was used to measure the fracture toughness (n = 6 per group). For these measurements, a V-notch was cut on a 3×36 mm^2 surface of the samples, with this surface placed under tension during the tests. The final V-notches in the samples were checked carefully, with depths of between 0.8 and 1.2 mm. Samples were tested via three-point bending with a crosshead speed of 1.0 mm/min and a span of 30 mm. The depth of the V-notches of the samples were read using a three-dimensional coordinate measuring system (SmartScope MVP 200, Quality Vision International, US) to give a_1, a_2 and a_3 values. The average notch depth (*a*, in metres) and the relative notch depth (*α*) were calculated using the following equations:

$$a = (a_1 + a_2 + a_3)/3 \tag{1}$$

$$\alpha = a/w \tag{2}$$

And, K_{Ic} was calculated using equation (3):

$$K_{Ic} = \frac{F}{b\sqrt{w}} \frac{S}{w} \frac{3\sqrt{\alpha}}{2(1-\alpha)^{1.5}} Y \tag{3}$$

where.

F is the fracture load (MN), *b* is the sample width (m), *w* is the sample thickness (m), *S* is the support span (m) and *Y* is the stress intensity shape factor.

In the measurements of the samples *S* is 30 mm and $S1/w = 7.5$, therefore:

$$Y = 1.964 - 2.837\alpha + 13.7714\alpha^2 - 23.250\alpha^3 + 24.129\alpha^4$$

The K_{Ic} data of the three groups show normality and homogeneity of variance, and analysis was conducted using one-way ANOVA, and LSD post hoc was used to make comparisons between the groups. All statistical analyses were performed using statistical software (IBM SPSS Statistics, v26.0; IBM Corp), $\alpha = 0.05$.

3. Results and discussion

3.1. Dimensional accuracy

Volume shrinkage can induce internal stress, which may lead to the deformation of the samples and a decrease in their precision [4]. Standard alternating x/y-raster scanning reduces the stress concentration and warpage more effectively than x or y scanning alone [2]. Compared with the theoretical dimensions, only the thickness of the group H samples shows no statistically significant difference, and the most significant difference is observed for the length of the U group samples (Table 1). These two dimensions correspond to the stacking height of the layers in the Z axis direction. This phenomenon indicates that a lower stacking height results in more accurate dimensions. From the scatter
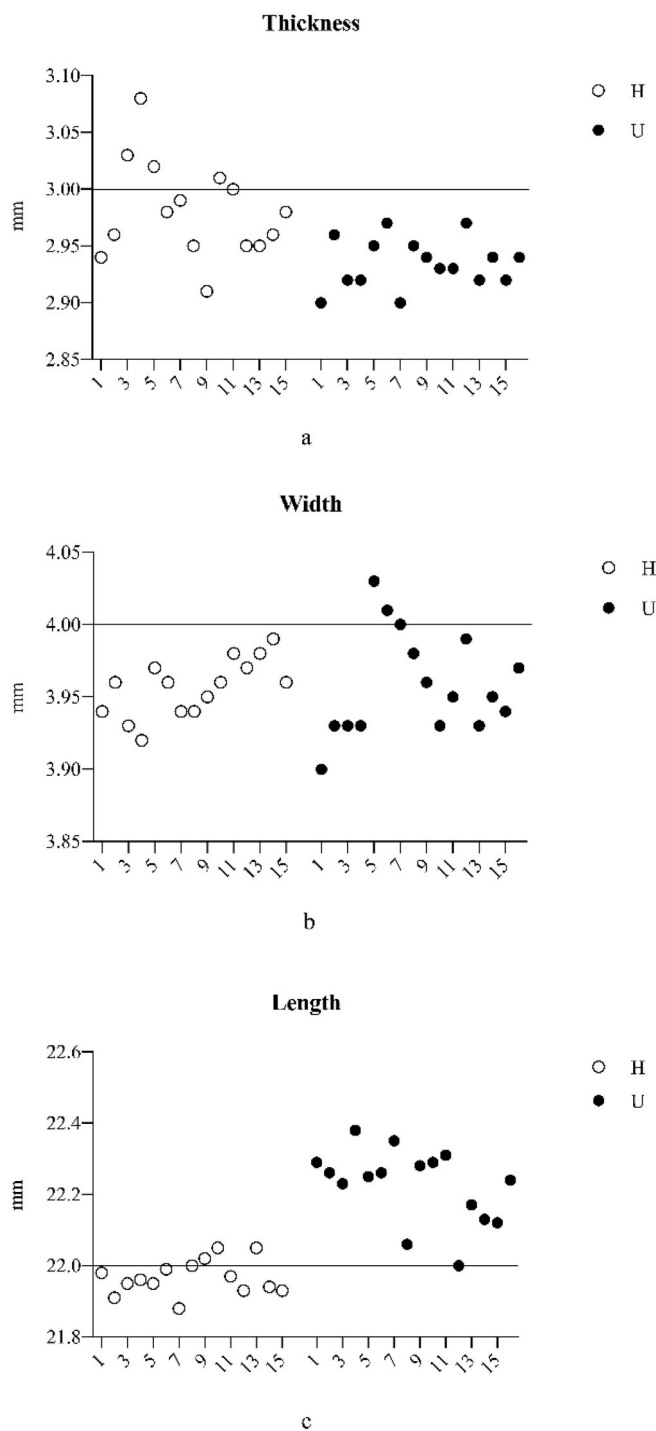
Thickness

a

Width

b

Length

c

Fig. 2. Scatter plots of the dimensions of the short bars of the samples: a: thickness; b: width; and c: length. The horizontal lines represent the theoretical values.

plots shown in Fig. 2, it can be seen that most of the data points are lower than the theoretical values, except for the thickness of the H samples (the points are distributed relatively evenly) and the length of the U samples (almost all the points are above the theoretical values). This indicates that during the sintering process, greater shrinkage occurs than expected in the XY direction. The variations in length are great, showing that the results are not reliable for large dimensions. The length of U is the only mean value that is greater than the theoretical value, suggesting that the shrinkage is lower than expected in the Z axis direction (layer stacking direction). It is speculated that low shrinkage contributes toward
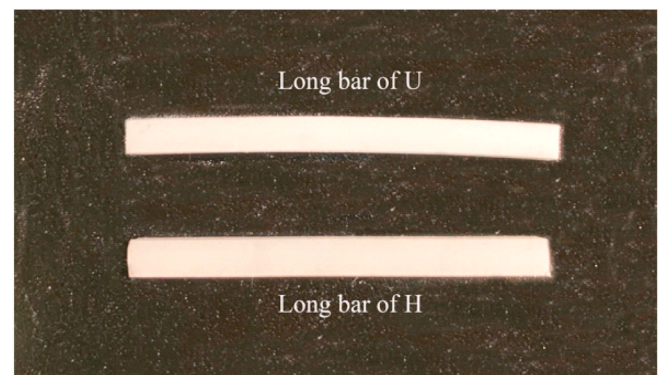

Fig. 3. Long bars of U and H group samples. The upper bar is a U sample and shows obvious warpage, and the lower bar is a H sample.
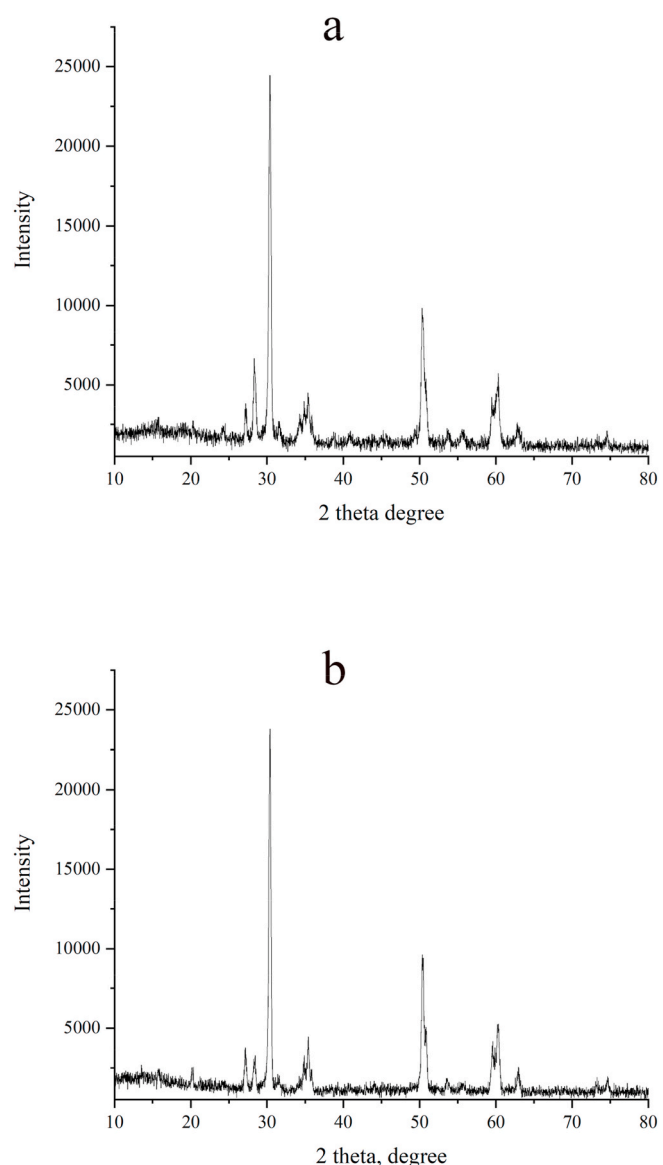

a

b

Fig. 4. X-ray diffraction patterns of a: H and b: U samples.

possible delamination and the occurrence of defects between successive layers. This phenomenon is magnified when the printing dimensions are large (22 mm). As for the thickness of H, a compromise between the high
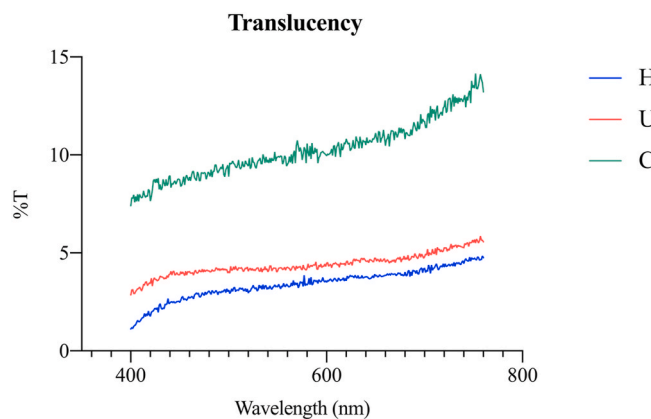
Fig. 5. Translucency measurements of H, U and C samples.

Table 2
Means and SD Ra values of the S1, S2 and S3 surfaces.

Group	Quantity	Ra (μm)
S1	8	0.71 (±0.10)[b]
S2	7	1.07 (±0.31)[a]
S3	6	1.09 (±0.08)[a]

The different superscripts represent statistically significant differences.

Fig. 6. Box plots of the roughness of surfaces S1, S2 and S3.

shrinkage and delamination of successive layers results in this value being equal to the theoretical value. This therefore indicates that the accuracy of printing does not meet clinical requirements, especially when the stacking height is made up of thick layers. However, these results provide a reference for improving printing accuracy. In clinical use, small dimensions of restoration materials to some extent ensure printing accuracy. Adjustment by grinding also allows the possibility of printing restorations for use in clinical applications. Some of the long bars in the U group of samples show visible warpage to the naked eye, whereas the long bars of the H group of samples and all of the short bars in the same group show no obvious warpage, as shown in Fig. 3. The warpage of AM ceramics mainly depends on the stress that arises between the layers [2]. The warpage observed in the long bars of the U group of samples can be attributed to large Z axis dimensions, leading to more contact between the layers, which results in high residual stress. In dentistry, the largest dimension of a monolithic crown is far lower than 36 mm or 22 mm, so warpage does not present a major problem. However, with clinical use in mind, 3–4 units bridges should be printed horizontally to create precise non-warped dental restorations. The null hypothesis that the accuracy of dimensions is the same in different orientations is rejected.

3.2. XRD, density and translucency measurements

The crystalline phases of the H and U samples are tetragonal, as shown in Fig. 4. The microstructure of the materials is the main factor that affects their optical properties, as pores cause light scattering and agglomerations densify and shrink independently of the matrix after heat treatment. This results in two outcomes: the formation of intragranular and intergranular pores and the elimination of intragranular pores, thereby leading to the formation of large grains in the materials [24]. Therefore, the internal defects in the samples, such as pores and agglomerations, have a negative effect on their optical properties. In this work, the layer height of the samples was 25 μm, as a small layer height helps to ensure that each layer is polymerised thoroughly, thereby preventing porosity and delamination issues from arising at the boundaries between the layers [28].

The theoretical density of 3 YSZ is 6.10 g/cm^3. The density of the H group samples (5.773 ± 0.025 g/cm^3, relative density 94.6%) is lower than that of the U group samples (5.818 ± 0.013 g/cm^3, relative density 95.4%). As shown in Fig. 5, the %T of the H, U and C groups are 3.403%, 4.393% and 10.253%, respectively. The U group samples have a higher density, which indicates that these samples contain fewer internal defects and therefore have a higher %T than the H group samples. Bar-shaped samples that are unequal in densities in the two build orientations (H and U) reveal a phenomenon that has not previously been observed. Bars of the U group samples have individual layers that exhibit a smaller area than those of bars of the H group samples, which may

indicate that a smaller layer area ensures more densification. Therefore, to improve %T, there is a requirement for denser parts with fewer internal defects. Another factor that influences translucency is surface roughness, but the surface conditions of the two groups are not identical for the sake of measuring the properties in the as-sintered condition in this test. Due to the lack of a standard by which to evaluate the quality of translucency of the samples, the %T values of traditional CAD/CAM discs, which were first mirror polished, were measured for comparison to the AM discs. The %T values of the C group samples are the highest and the translucency of the AM zirconia in that group is far below clinical requirements. In clinical treatment, grinding, polishing and glazing are essential, which are used to promote the optical and aesthetic properties of zirconia. Appropriate treatments of AM zirconia while improving its density improve the feasibility of its use in clinical applications. Therefore, the null hypothesis that there is no difference in translucency between the two build orientations is rejected.

3.3. Surface quality

The surface roughness values of the samples in this work are shown in Table 2 and Fig. 6, with the morphologies shown in Fig. 7. The morphology of S1 (Fig. 7 a) is relatively smooth, and it has the lowest surface roughness, reflecting the condition of the as-sintered surface of a single layer without any damage. S2 has a comparable surface roughness to that of S3, but with a relatively higher variance. This result shows that the manual defects of S2 are not homogeneous, as shown in Fig. 7 b and c. The uniform ripple-like patterns on S3, shown in Fig. 7 d and e, are formed as a "step effect", which might be the characteristic structure in
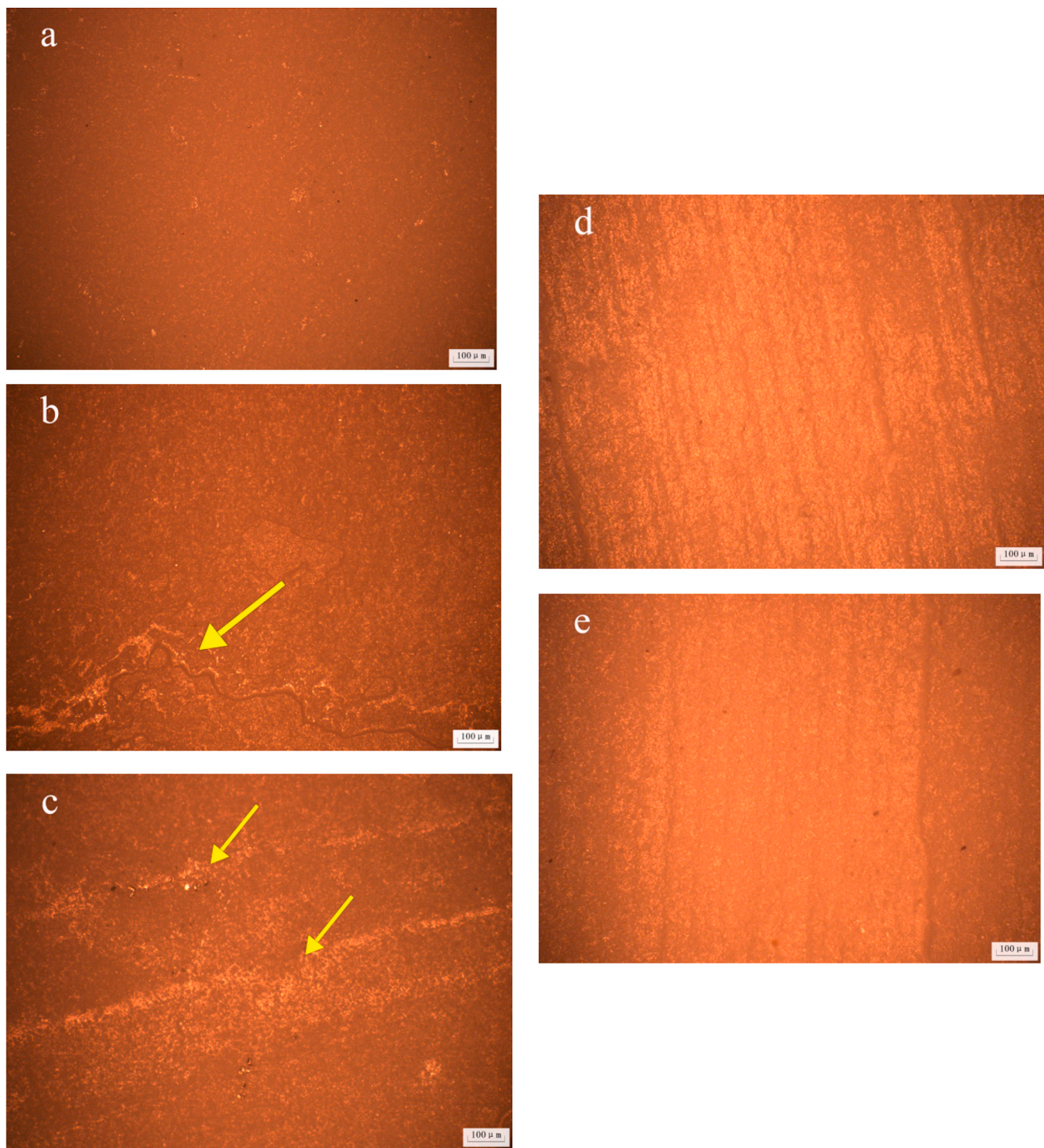
Fig. 7. Surface morphologies, a: S1, relatively smooth; b and c: irregular defects on S2; d and e: uniform ripple-like patterns on the two opposite S3.

the layer-by-layer stacking process [2,29].

3.4. Flexural strength measurements, fracture surface observations and Weibull statistics

The grouping and naming of the short bars are listed in the appendix. The flexural strength of the original H group samples is shown in Table 3 and Fig. 8a. From the results, it can be seen that there are no significant differences between H1 and H2, but there is an increase in the flexural strength of the Polished-H samples. In most cases, the materials strength

data reported in the literature or that listed on the property data sheets provided by manufacturers represent the maximum strength achievable using well-polished components [30]. However, SLA is a near-net sha-ped technique, wherein the surface morphologies and strengths of the components in the as-sintered SLA ceramics are essential for predicting their reliability when used in dental restorations. Different values of the threshold of the surface roughness that inhibits bacterial adherence have been reported in the literature [31,32]. However, even compared with the highest acceptable roughness value ($R_a < 0.58$ μm) [32], the R_a values of the three types of AM zirconia, including surfaces of H with and

Table 3

Means, SD flexural strengths (σ), Weibull moduli and Weibull characteristic strengths of the samples in this work.

Primary groups	Groups		Quantity	σ (MPa)	Weibull moduli	Weibull characteristic strength (MPa)
Original H groups	As–H	H1	8	895.43 (±174.96)[b]	6.50	920.22
		H2	7	817.36 (±108.91)[b]		
	Polished-H		6	1095.94 (±200.98)[a]		
Modified H groups	HC1		5	966.97 (±98.61)[b]		
	HC2		3	910.38 (±42.87)[bc]		
	Polished-HC		5	1151.08 (±166.41)[a]		
	HD		8	767.40 (±138.25)[c]		
U	As–U		16	206.73 (±31.00)[a]	7.99	219.59
	Polished-U		4	225.44 (±46.10)[a]		

The different superscripts represent statistically significant differences in the individual primary groups.

without manual defects and surfaces of U, are still too high (the minimum R_a is 0.71 μm), which means that bacteria can accumulate on their surfaces, thereby simultaneously increasing the risk of secondary caries and periodontal inflammation if these materials were to be used in dental restoration. A rough surface also causes wear of antagonist enamel [33]. Therefore, it is essential for the AM zirconia to be polished to reduce the accumulation of bacteria and antagonist wear. As for flexural strength of the AM zirconia, there is no statistically significant difference between the H1 and H2 samples, but the strengths of both are lower than that of the Polished-H sample. This signifies that a smooth surface without any defects significantly improves the strength of the material. However, this does not mean that as-sintered AM zirconia with a rough surface is meaningless. A uniform and rough surface morphology may also be used to directly enhance bonding between ceramic restorations and teeth or between the substrate and the veneer layer of the teeth. However, there have been few studies on bonding tests.

The H1, H2 and Polished-H samples exhibit two fracture modes after three-point bending tests: fracture from the stress concentration area (HC, Fig. 9 a) and splintering due to crack deflection (HD, Fig. 9 b). HC can be classified into three modified groups according to the different fracture modes and surface conditions in the three-point bending tests: as-sintered S1 and S2 samples (HC1 and HC2), and 2000 diamond polished samples (Polished-HC). The flexural strength of the four modified groups (HC1, HC2, Polished-HC and HD) was analysed, with the results shown in Table 3 and Fig. 8 b. The Polished-HC exhibits the highest flexural strength amongst the samples, with a value of 1151.08 ± 166.41 MPa. The flexural strengths of HC1 and HC2 are the same, but both samples exhibit lower values than that of the Polished-HC. HD exhibits the lowest flexural strength. In the three-point bending tests, the upper part of the bar is shortened under compression, and the lower part is extended under tension. The layer in the middle is neither in compression nor tension and thus maintains its original length. This layer is called the neutral surface and suffers the largest shear force as it is the critical surface between the compression and tension parts. On the fracture surface of HC, shown in Fig. 10 a and b, transverse cracks can be observed, with their location near or corresponding to the neutral surface that experiences the greatest shear force. This result indicates that there is weak bonding between the successive layers and shows that the bond strength cannot resist the shear force during the three-point bending measurements. However, there is another possibility that delamination has already occurred in the middle of the samples, as it is difficult to heat the middle thoroughly and uniformly, but these conjectures need to be further confirmed. The crack propagation direction of HD is not parallel to the load direction but instead oblique to it (Fig. 10 c), indicating that internal defects arise as the material brittle and is thus prone to defects. When a crack propagates to the middle of a sample, the crack deflects to the long axis and contributes towards the large shear force near the neutral surface or the delamination that already exists. Amongst the samples, HD exhibits the lowest flexural strength, signifying that its internal defects are a major problem that reduces its flexural strength during testing. The Polished-HC has a

higher flexural strength than both HC1 and HC2, showing that producing a smoother surface without surface defects can improve the flexural strength of samples without the formation of severe internal defects. The flexural strength of HC1 is higher than that of HC2, but with no statistically significant difference. There are two reasons for this: (1) small defects could also exist on the as-sintered surfaces and reduce flexural strength due to the technical limitations of SLA; (2) the number of samples of HC2 is not large enough (n = 3), which may lead to inaccurate results. Above all, factors that influence the flexural strength of horizontally printed zirconia are not single but double, including both internal and surface defects. Therefore, even though H1 and H2 show no difference in flexural strength, it can still not be concluded that manual defects do not affect flexural strength. However, after considering internal defects and surface conditions, a comparison between HC1 and HC2 supports the null hypothesis that manual defects have no effect on the flexural strength of AM zirconia, but further testing of a sufficient number of samples should be conducted for verification.

There is no statistically significant difference in flexural strength between the As–U (206.73 ± 31.00 MPa) and Polished-U (225.44 ± 46.10 MPa) samples. The U group of samples has a higher density than the H group, but a comparison of the flexural strength revealed the opposite trend. One reason for this is that the uprightly printed samples have layers that are parallel to the applied force [19]. This indicates that the bonding between the layers is not strong enough compared to the bonding within a single layer [17,34]. The flexural strengths of the samples printed in an upright fashion before and after polishing are the same. This phenomenon also supports the conclusion that adhesion between adjacent layers is insufficient and that the impact that surface conditions has on flexural strength is not obvious. According to a previous study, slightly ripple-like structural features indicate that layers are tightly sintered into a whole body [29]. However, the ripple-like structure of U in this study is distinct, as shown in Fig. 7 d and e, with this phenomenon being an indication of the weak combination of layers. It should be noted that flaws such as surface defects, pores and agglomerations, shown in Fig. 10 e, f and g are inevitable. These flaws increase the risk of reducing the strength of AM zirconia, but not completely. Therefore, grinding, polishing and glazing are essential, not only to promote the optical and aesthetic properties of zirconia, but also to reduce its surface defects to improve its flexural strength and reliability.

Delamination can be observed between the layers in the HD and U samples, as shown in Fig. 10 c and d. Representative flaws of AM zirconia are shown in Fig. 10 e, f and g, which correspond to the pores of HC, and agglomerations and surface defects of U, respectively. These three types of flaws may exist on any type of sample.

Weibull statistical analysis was conducted to evaluate the structural reliability of AM zirconia. The Weibull characteristic strength is the strength that occurs at a probability of failure of 63.2% for a particular test sample and loading configuration. The Weibull modulus is the parameter that describes the shape of the distribution of strength as a function of the failure probability. The smaller the Weibull modulus, the larger the scattering of the data. There is no statistically significant
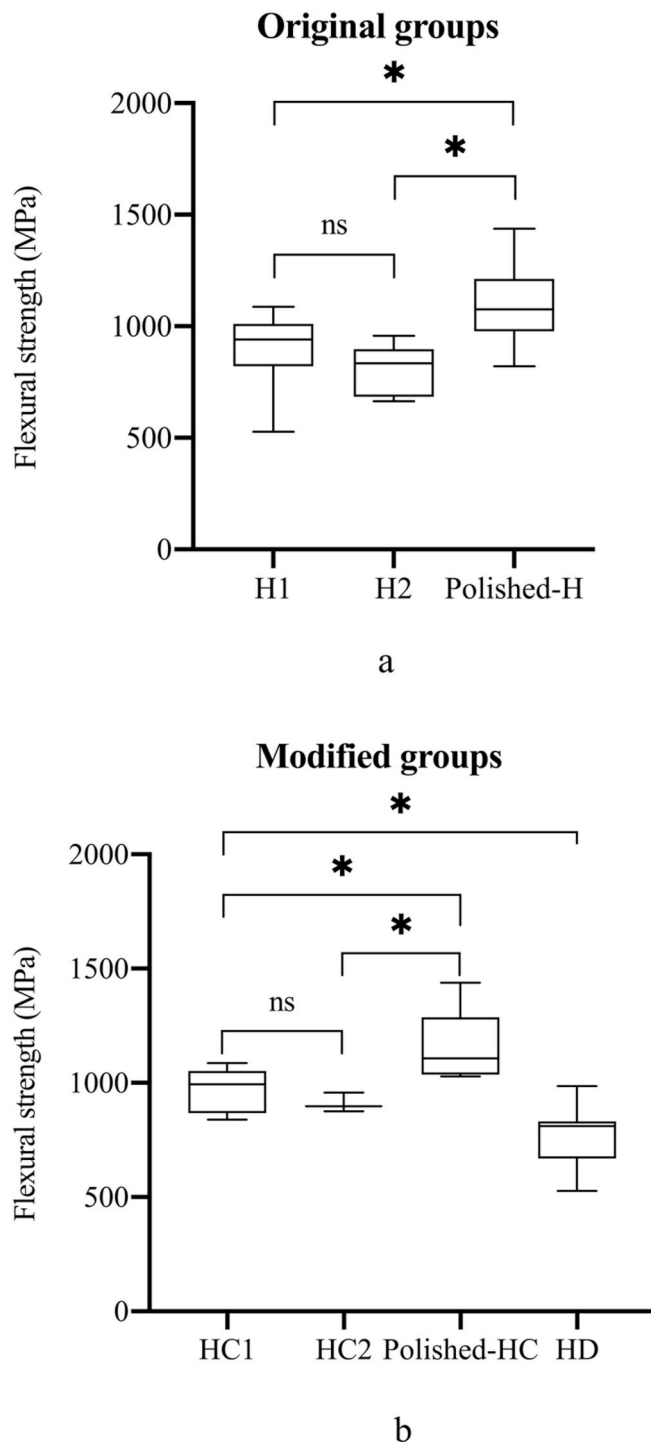
Original groups

a

Modified groups

b

Fig. 8. Box plots of flexural strength. a: original groups and b: modified groups. The asterisks represent statistically significant difference.

difference in the flexural strength between H1 and H2, therefore the flexural strength data of As–H were used for Weibull statistical analysis. The Weibull characteristic strength and moduli of As–H are 920.22 MPa and 6.50 and of As–U are 219.59 MPa and 7.99, respectively (Fig. 11). As–H has greater Weibull characteristic strength than As–U. The Weibull characteristic strength is often more fit for representing the strength of ceramics. As–H has a smaller Weibull modulus, which indicates a larger scattering of the data.

It should be emphasised that in AM ceramics weak bonding between adjacent layers is a common issue [29,35,36]. One speculation for this is
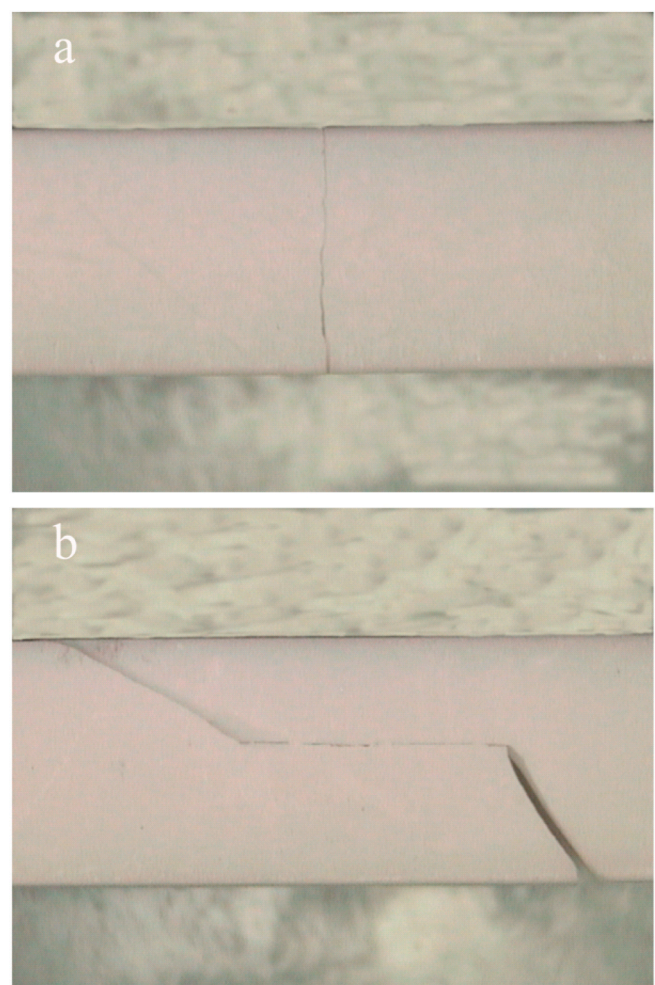

Fig. 9. Two fracture modes: a: fracture from a stress concentration area and b: splintering due to crack deflection.

that metals are segregated at the bottom of each monolayer suspension during the SLA process, making the upper zone of the monolayer poorer in metal elements, which is associated with more critical shrinkage and less efficient sintering [37]. However, this speculation needs more confirmation, and the weak bonding in adjacent layers is still a problem that has not yet been properly solved.

3.5. Fracture toughness

The indentation method is commonly used for testing fracture toughness, as it is simple and convenient. This method can be used to directly compare the fracture toughness of different materials under the same test conditions, but calculated values do not accurately reflect the fracture toughness of zirconia. The SEVNB method is recommended for carrying out ceramic fracture toughness tests, in accordance with ISO 23146 [38]. Although, it is difficult for yttria tetragonal polycrystalline zirconia to form a sharp notch-tip radius, resulting in the SEVNB method not being suitable for zirconia [39]; therefore, a V-notch was carefully made in the samples in this study. The K_{Ic} values of the H, U and C groups are 12.635 ($\pm$1.372) MPa·m$^{1/2}$, 9.276 ($\pm$1.004) MPa·m$^{1/2}$ and 14.721 ($\pm$0.974) MPa·m$^{1/2}$, with significant differences. The H Group exhibits significantly higher K_{Ic} values than those of the U group, indicating that the H group better prevents crack growth. The reason for this may be similar to that for different flexural strengths being exhibited between samples with two orientations: the V-notch and force direction are perpendicular to the layers in the H group of samples, but parallel to the layers in the U group of samples. However, all of the values are
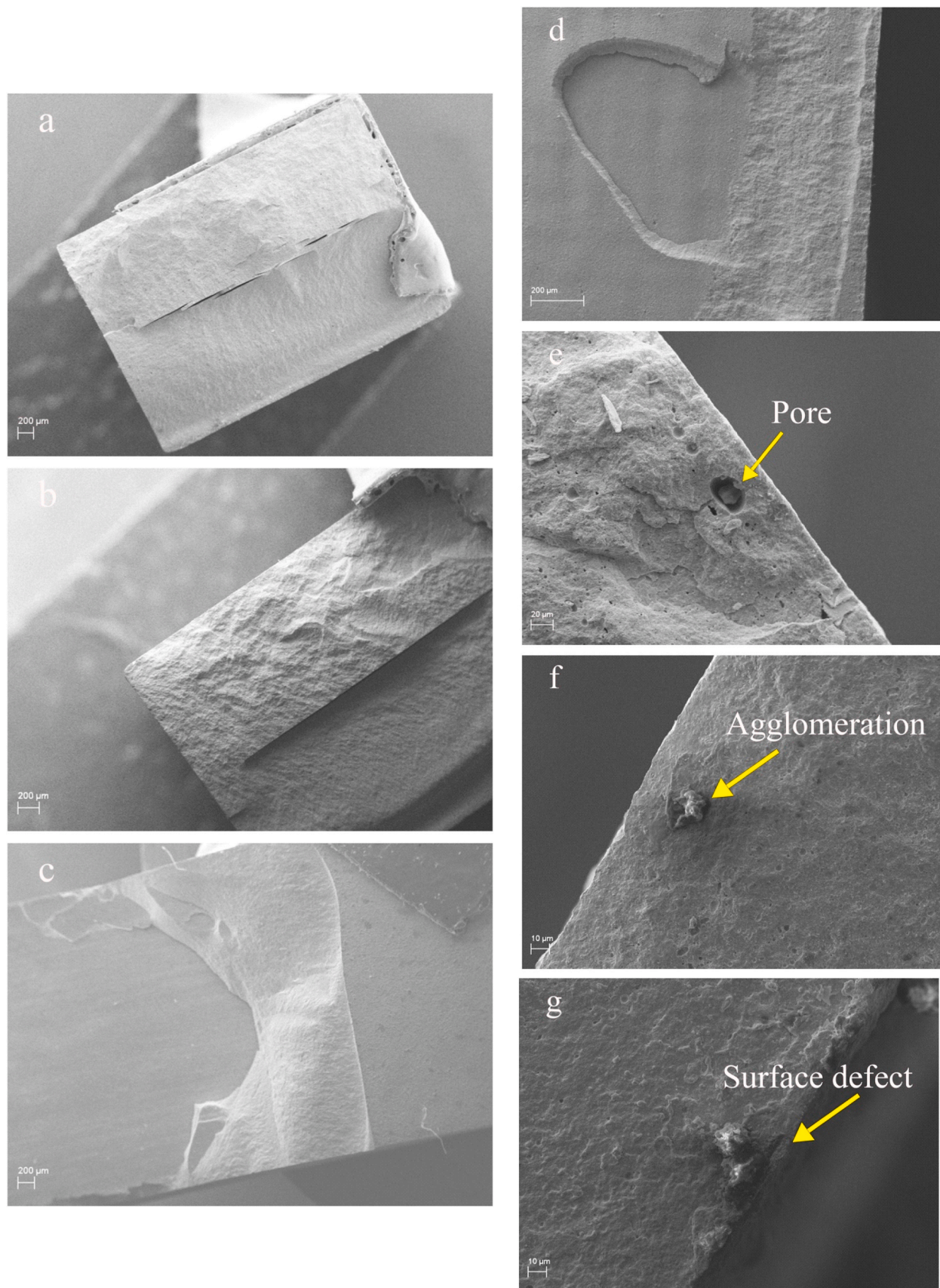
Fig. 10. SEM observations of fractured surfaces. a and b: HC; c: HD; d: U; e: pore of HC; f and g: agglomeration and surface defect of U.
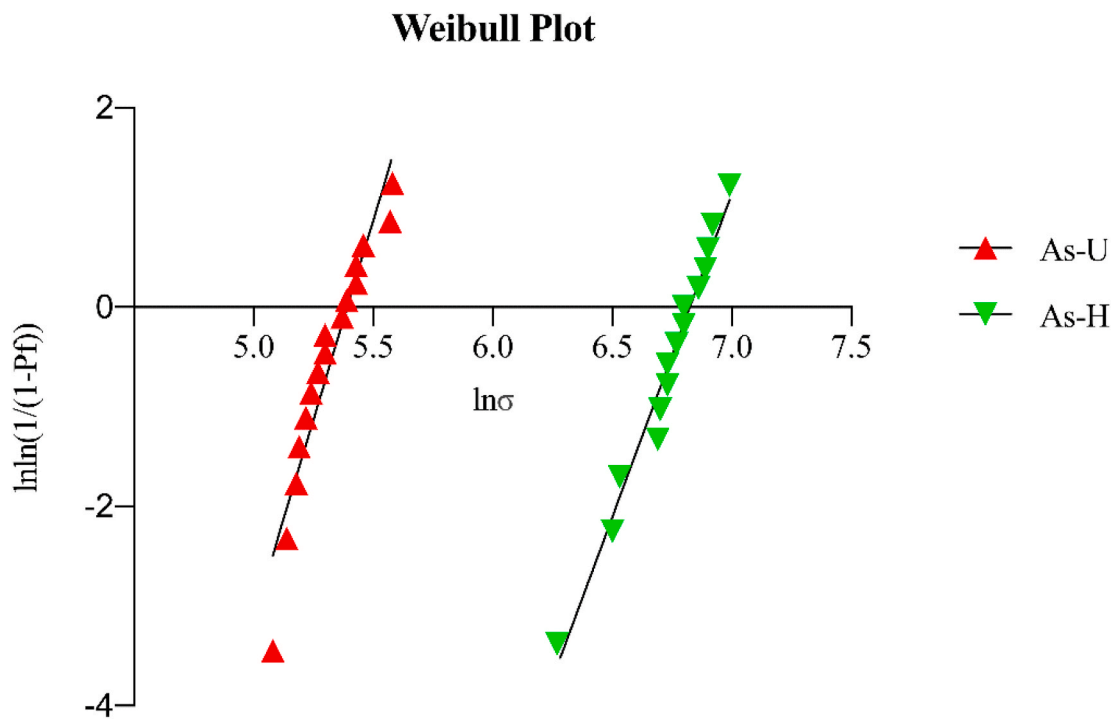
Weibull Plot

Fig. 11. Weibull plots of the As–H and As–U groups.

greater than the highest required value (5 MPa m$^{1/2}$) for a material to be used in dental applications [39]. Therefore, the null hypothesis that there are no differences in mechanical properties between two build orientations is rejected.

Due to the constraints of blade thickness when making notches, a submicron sharp V-notch is extremely hard to achieve, which may be problematic for fracture toughness testing in fine-grained ceramics if the notch root radius is larger than 1.5- to 3-fold the average grain size [40]. Therefore, the K$_{Ic}$ values in this work are not guaranteed to be totally accurate. Compared with the K$_{Ic}$ values reported in previous studies, the values in this test are obviously higher [40–43]. 3 YSZ prepared using a femtosecond laser and focused ion beam milling exhibits an ultra-sharp V-notch and K$_{Ic}$ values of 4.4 and 5.64 MPa m$^{1/2}$, respectively, values that are lower than the acquired results in this study [40,43]. This may be due to the notch-tip radius not being sharp, even though the V-notch was carefully made, which is a limitation of this study. However, the conclusion can still be drawn that the H group of samples has higher K$_{Ic}$ values than the U groups of samples, as the preparation and test conditions are the same between the two groups. Considering that the K$_{Ic}$ values of the AM samples are relatively high, the K$_{Ic}$ values of CAD/CAM samples acquired using the same method were evaluated for comparison. The C group samples exhibit the highest K$_{Ic}$ values and the lowest standard deviation amongst all the groups, indicating that CAD/CAM zirconia better prevents crack growth than AM zirconia. However, grain size and K$_{Ic}$ data should be measured using other testing methods for further verification.

Horizontally printed samples exhibit excellent mechanical properties as the load direction is perpendicular to the layers, and they have better dimensional accuracy and a shorter manufacturing time as a result of the lower stacking height of the layers. However, conclusions cannot be drawn that objects in this build direction are suitable for use in clinical applications. Simple shaped samples are essential and appropriate for measuring the basic properties of a material. However, the complex shapes of dental restorations and the masticatory stresses in the oral environment cannot be simulated using simple shaped samples and tests. Therefore, tests should be carried out under conditions that are closer to the real masticatory stress distribution with complex-shaped

objects to evaluate the prospects of the use of AM zirconia in clinical applications.

The flexural strength of the As–H and Polished-H samples meet the requirements for prostheses with four or more units according to ISO 6872–2015, whereas the As–U and Polished-U samples are only suitable for producing single unit prostheses [39]. Considering masticatory stresses are experienced from different directions, printed zirconia restorations should be used according to their minimum strength. In this study, considering accuracy and strength, it was found that printed zirconia can be applied for producing single unit prostheses for use in dentistry.

4. Conclusions

It was found that dimensional accuracy, translucency and mechanical properties vary in different build orientations. Zirconia printed in an upright fashion has a higher density and translucency than horizontally printed zirconia. However, horizontally printed zirconia exhibits excellent accuracy and mechanical properties. Stress and weak bonding strength among the successive layers of the materials in this study are the main issues that need to be solved. Manual surface defects that arise as a result of the process of separating objects from the build platform not only affect the appearance of an object, but also increase the risk of its failure. Internal flaws in objects, such as pores and agglomerations, hinder the formation of a dense part and have negative effects on its translucency and mechanical properties.

It was found in this study that AM zirconia can be applied in single unit dental prostheses and shows excellent prospects for use in dental applications, but further tests, in which the conditions better mimic those of actual clinical applications, are needed to prove their reliability. The next key goal is to tightly sinter the successive layers of zirconia to form a whole part for the purpose of improving the flexural strength of samples that are printed in an upright fashion. It is possible that printed zirconia could be applied in dental prostheses that have more units with higher bonding strength between their adjacent layers. However, whether the as-sintered surfaces could be used to bond to teeth and veneer also needs to be tested.

References

[1] J. Schweiger, D. Bomze, M. Schwentenwein, 3D printing of zirconia–what is the future? Current Oral Health Reports 6 (2019) 339–343.

[2] H. Xing, B. Zou, S. Li, X. Fu, Study on surface quality, precision and mechanical properties of 3D printed ZrO2 ceramic components by laser scanning stereolithography, Ceram. Int. 43 (2017) 16340–16347.

[3] J.R. Strub ., E.D. Rekow, S. Witkowski, Computer-aided design and fabrication of dental restorations: current systems and future possibilities, J. Am. Dent. Assoc. 137 (2006) 1289–1296.

[4] H. Quan, T. Zhang, H. Xu, S. Luo, J. Nie, X. Zhu, Photo-curing 3D printing technique and its challenges, Bioact Mater 5 (2020) 110–115.

[5] K.B. Kim, J.H. Kim, W.C. Kim, J.H. Kim, Three-dimensional evaluation of gaps associated with fixed dental prostheses fabricated with new technologies, J. Prosthet. Dent 112 (2014) 1432–1436.

[6] L.N. Hoang, G.A. Thompson, S.H. Cho, D.W. Berzins, K.W. Ahn, Die spacer thickness reproduction for central incisor crown fabrication with combined computer-aided design and 3D printing technology: an in vitro study, J. Prosthet. Dent 113 (2015) 398–404.

[7] Y. Kajima, A. Takaichi, T. Nakamoto, T. Kimura, Y. Yogo, M. Ashida, H. Doi, N. Nomura, H. Takahashi, T. Hanawa, N. Wakabayashi, Fatigue strength of Co-Cr-Mo alloy clasps prepared by selective laser melting, J Mech Behav Biomed Mater 59 (2016) 446–458.

[8] N. Kittikundecha, Y. Kajima, A. Takaichi, H.H. Wai Cho, H.L. Htat, H. Doi, H. Takahashi, T. Hanawa, N. Wakabayashi, Fatigue properties of removable partial denture clasps fabricated by selective laser melting followed by heat treatment, J Mech Behav Biomed Mater 98 (2019) 79–89.

[9] A. Cheng, A. Humayun, B.D. Boyan, Z. Schwartz, Enhanced osteoblast response to porosity and resolution of additively manufactured Ti-6Al-4V constructs with trabeculae-inspired porosity, 3D Print. Addit. Manuf. 3 (2016) 10–21.

[10] M. Revilla-Leon, L. Ceballos, I. Martinez-Klemm, M. Ozcan, Discrepancy of complete-arch titanium frameworks manufactured using selective laser melting and electron beam melting additive manufacturing technologies, J. Prosthet. Dent 120 (2018) 942–947.

[11] K. Takahashi, M. Torii, T. Nakata, N. Kawamura, H. Shimpo, C. Ohkubo, Fitness accuracy and retentive forces of additive manufactured titanium clasp, J Prosthodont Res 64 (2020) 468–477.

[12] R. Ramakrishnaiah, A.A. Al Kheraif, A. Mohammad, D.D. Divakar, S.B. Kotha, S. L. Celur, M.I. Hashem, P.K. Vallittu, I.U. Rehman, Preliminary fabrication and characterization of electron beam melted Ti-6Al-4V customized dental implant, Saudi J. Biol. Sci. 24 (2017) 787–796.

[13] H. Li, L. Song, J. Sun, J. Ma, Z. Shen, Stereolithography-fabricated zirconia dental prostheses: concerns based on clinical requirements, Adv. Appl. Ceram. 119 (2020) 236–243.

[14] G. Mitteramskogler, R. Gmeiner, R. Felzmann, S. Gruber, C. Hofstetter, J. Stampfl, J. Ebert, W. Wachter, J. Laubersheimer, Light curing strategies for lithography-based additive manufacturing of customized ceramics, Additive Manufacturing 1–4 (2014) 110–118.

[15] J.-H. Kim, W.-Y. Maeng, Y.-H. Koh, H.-E. Kim, Digital light processing of zirconia prostheses with high strength and translucency for dental applications, Ceram. Int. 46 (2020) 28211–28218.

[16] C.-J. Bae, J.W. Halloran, Influence of residual monomer on cracking in ceramics fabricated by stereolithography, Int. J. Appl. Ceram. Technol. 8 (2011) 1289–1295.

[17] A. Zocca, P. Colombo, C.M. Gomes, J. Günster, D.J. Green, Additive manufacturing of ceramics: issues, potentialities, and opportunities, J. Am. Ceram. Soc. 98 (2015) 1983–2001.

[18] A.C. Branco, R. Silva, H. Jorge, T. Santos, K. Lorenz, M. Polido, R. Colaço, A. P. Serro, C.G. Figueiredo-Pina, Tribological performance of the pair human teeth vs 3D printed zirconia: an in vitro chewing simulation study, J. Mech. Behav. Biomed. Mater. 110 (2020).

[19] R.B. Osman, A.J. van der Veen, D. Huiberts, D. Wismeijer, N. Alharbi, 3D-printing zirconia implants; a dream or a reality? An in-vitro study evaluating the dimensional accuracy, surface topography and mechanical properties of printed zirconia implant and discs, J Mech Behav Biomed Mater 75 (2017) 521–528.

[20] W. Oropallo, L.A. Piegl, Ten challenges in 3D printing, Eng. Comput. 32 (2015) 135–148.

[21] W. Wang, H. Yu, Y. Liu, X. Jiang, B. Gao, Trueness analysis of zirconia crowns fabricated with 3-dimensional printing, J. Prosthet. Dent 121 (2019) 285–291.

[22] Y. Lu, Z. Mei, Y. Lou, L. Yue, X. Chen, J. Sun, Z. Wan, H. Yu, Schwickerath adhesion tests of porcelain veneer and stereolithographic additive-manufactured zirconia, Ceram. Int. 46 (2020) 16572–16577.

[23] W. Harrer, M. Schwentenwein, T. Lube, R. Danzer, Fractography of zirconia-specimens made using additive manufacturing (LCM) technology, J. Eur. Ceram. Soc. 37 (2017) 4331–4338.

[24] R. Shahmiri, O.C. Standard, J.N. Hart, C.C. Sorrell, Optical properties of zirconia ceramics for esthetic dental restorations: a systematic review, J. Prosthet. Dent 119 (2018) 36–46.

[25] Q. Lian, X. Wu, D. Li, X. He, J. Meng, X. Liu, Z. Jin, Accurate printing of a zirconia molar crown bridge using three-part auxiliary supports and ceramic mask projection stereolithography, Ceram. Int. 45 (2019) 18814–18822.

[26] R. Li, Y. Wang, M. Hu, Y. Wang, Y. Xv, Y. Liu, Y. Sun, Strength and adaptation of stereolithography-fabricated zirconia dental crowns: an in vitro study, Int. J. Prosthodont. (IJP) 32 (2019) 439–443.

[27] C. Kolb, K. Gumpert, H. Wolter, G. Sextl, Highly translucent dental resin composites through refractive index adaption using zirconium dioxide nanoparticles and organic functionalization, Dent. Mater. 36 (2020) 1332–1342.

[28] J. Deckers, J. Vleugels, J.P. Kruthl, Additive manufacturing of ceramics: a review, J. Ceram. Sci. Tech. 5 (2014) 245–260.

[29] D. An, W. Liu, Z. Xie, H. Li, X. Luo, H. Wu, M. Huang, J. Liang, Z. Tian, R. He, A strategy for defects healing in 3D printed ceramic compact via cold isostatic pressing: sintering kinetic window and microstructure evolution, J. Am. Ceram. Soc. 102 (2019) 2263–2271.

[30] Z. Shen, L. Liu, X. Xu, J. Zhao, M. Eriksson, Y. Zhong, E. Adolfsson, Y. Liu, A. Kocjan, Fractography of self-glazed zirconia with improved reliability, J. Eur. Ceram. Soc. 37 (2017) 4339–4345.

[31] C.M. Bollen, P. Lambrechts, M. Quirynen, Comparison of surface roughness of oral hard materials to the threshold surface roughness for bacterial plaque retention: a review of the literature, Dent. Mater. 13 (1997) 258–269.

[32] M. Zhang, Z. Zhang, N. Ding, D. Zheng, Effect of airborne-particle abrasion of presintered zirconia on surface roughness and bacterial adhesion, J. Prosthet. Dent 113 (2015) 448–452.

[33] K. Tachibana, I. Atsuta, Y. Tsukiyama, R. Kuwatsuru, T. Morita, H. Yoshimatsu, Y. Matsushita, I. Narimatsu, Y. Ayukawa, Y. Sawae, K. Koyano, The Need for Polishing and Occlusal Adjustment of Zirconia Prostheses for Wear on Antagonist Teeth, Dent Mater J, 2021.

[34] H. Li, L. Song, J. Sun, J. Ma, Z. Shen, Dental ceramic prostheses by stereolithography-based additive manufacturing: potentials and challenges, Adv. Appl. Ceram. 118 (2018) 30–36.

[35] M. Dehurtevent, L. Robberecht, A. Thuault, E. Deveaux, A. Leriche, F. Petit, C. Denis, J.C. Hornez, P. Béhin, Effect of build orientation on the manufacturing process and the properties of stereolithographic dental ceramics for crown frameworks, J. Prosthet. Dent 125 (2021) 453–461.

[36] H. Wu, W. Liu, L. Lin, L. Li, Y. Li, Z. Tian, Z. Zhao, X. Ji, Z. Xie, S. Wu, Preparation of alumina-toughened zirconia via 3D printing and liquid precursor infiltration: manipulation of the microstructure, the mechanical properties and the low temperature aging behavior, J. Mater. Sci. 54 (2019) 7447–7459.

[37] A. Greco, A. Licciulli, A. Maffezzoli, Stereolithography of ceramic suspensions, J. Mater. Sci. 36 (2001) 99–105.

[38] International Organization for Standardization, ISO 23146:2012, Fine Ceramics (Advanced Ceramics, Advanced Technical Ceramics) — Test Methods for Fracture Toughness of Monolithic Ceramics — Single-Edge V-Notch Beam (SEVNB) Method.

[39] International Organization for Standardization, ISO 6872:2015, Dentistry — Ceramic Materials.

[40] H. Liu, W. Zhao, Y. Ji, J. Cui, Y. Chu, P. Rao, Determination of fracture toughness of zirconia ceramics with different yttria concentrations by SEVNB method, Ceram. Int. 43 (2017) 10572–10575.

[41] Z. Mei, Y. Lu, Y. Lou, P. Yu, M. Sun, X. Tan, J. Zhang, L. Yue, H. Yu, Determination of hardness and fracture toughness of Y-TZP manufactured by digital light processing through the indentation technique, BioMed Res. Int. 2021 (2021) 6612840.

[42] J.U. Jansen, N. Lumkemann, B. Sener, B. Stawarczyk, Comparison of fracture toughness measurements for zirconia materials using two test methods, Dent. Mater. J. 38 (2019) 806–812.

[43] Y. Liao, M. Gruber, H. Lukic, S. Chen, S. Megremis, Fracture toughness of zirconia with a nanometer size notch fabricated using focused ion beam milling, J. Biomed. Mater. Res. B Appl. Biomater. 108 (2020) 3323–3330.